Conf-9304166--1

LA-UR-93-2339

Title: **A REVIEW OF THE STAGES OF WORK HARDENING**

Author(s): A. D. Rollett, MST-6
U. F. Kocks, CMS

Submitted to: Proceedings of "DISLOCATIONS-93" Conference held at Aussois, France, April 1-9, 1993; to be published in the Materials Science Forum

Los Alamos
NATIONAL LABORATORY

A REVIEW OF THE STAGES OF WORK HARDENING

A. D. Rollett, U. F. Kocks

KEYWORDS: WORK HARDENING; STRESS; STRAIN; STRAIN RATE SENSITIVITY; STAGE IV; TEMPERATURE

ABSTRACT

The stages of work hardening are reviewed with an emphasis on the links between each stage. Simple quantitative descriptions are given for each stage, where possible. The similarities between stage I, easy glide, and stage IV, large strain hardening, are pointed out both in terms of the magnitude of the hardening rate, and in terms of the underlying mechanism of dislocation debris accumulation. Stage II is described as an athermal hardening stage that occurs when statistical variations in the dislocation "forest" lead to geometrical storage of dislocations. The steadily decreasing hardening rate observed in stage III is characterized by the increasing rate of loss of dislocation density due to dynamic recovery. Stage III appears to have an asymptote to a saturation stress which is determined by the characteristics of the dislocation tangles, or cell walls. The imperfect nature of the dynamic recovery process, however, leads to the accumulation of dislocation debris and this, by analogy with stage I, causes the apparent saturation stress to rise, thus causing stage IV.

INTRODUCTION

By 1956, a large amount of research into the mechanical properties of single crystals led Diehl [1] to divide the stress-strain curve into three stages, figure 1. Stage I occurs only during single slip in single crystals. Stage II is a linear hardening stage with a relatively high work hardening rate and occurs in both single crystals and polycrystals, independently of stage I. This hardening behavior is best thought of as a limiting behavior at small strains since the extent to which it is observed decreases with increasing temperature and stacking fault energy.

Stage III corresponds to a steady decrease of work hardening rate and is sensitive to temperature and strain rate. The theory for stage III discussed below assumes that a

saturation stress is reached at the end of stage III when recovery balances dislocation storage. When this discussion turns to consideration of large strain behavior, a further stage IV must be added, however. This stage is the low level work hardening that persists in some cases to very large strains. The existence of a stage IV in work hardening requires modification of any theory of stage III that predicts saturation of the flow stress at the end of stage III. Some authors refer to a stage V during which further dynamic recovery takes place, leading to an eventual actual saturation of the flow stress. This repeated dynamic recovery can be analysed with the same kinetics as for stage III, Gil-Sevillano [2].

Stage IV as discussed here is usually thought of as the small but sustained hardening that occurs at very large strains, e.g. as observed in wire-drawing of iron by Langford and Cohen [3]. The experimental evidence reviewed below strongly suggests that the persistent hardening at large strains is a real phenomenon in various metals and alloys and in various straining paths. This is the behavior to which the term stage IV is now generally applied, even if the hardening does not remain constant. It is only significant, however, at low homologous temperatures as evidenced by the large body of literature on creep plasticity which demonstrates the existence of a saturation stress under many different conditions of loading and temperature.

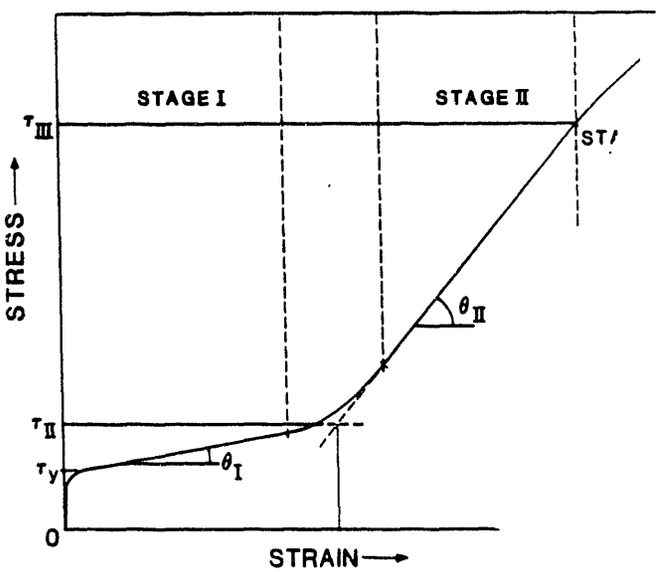

Fig. 1 The Stages of Work Hardening after Diehl, stage I/Easy Glide, stage II/Athermal Work Hardening and stage III/Dynamic Recovery.

The various stages of work hardening are most clearly distinguished on a diagram of θ versus σ, where $\theta=d\sigma/d\varepsilon$, figure 2. The discussion of stress and strain resolved onto a single, equivalent slip system (τ and γ, respectively) is given later: for now, we simply state that $\sigma=<M>\tau$ and $\gamma=<M>\varepsilon$, where <M> is the average Taylor factor for a polycrystal and is a function of deformation history but whose value is typically close to 3. Stage II is commonly found in single crystal experiments on low stacking fault energy materials and at low temperature at a constant, high, value of θ at about $\mu/200$ ($d\tau/d\gamma$). Even when not present, as in most cases of polycrystal experiments, stage II is

still useful as an asymptotic value of the hardening rate obtained by extrapolating the data back to the yield stress (zero strain). Stage III can often be represented by a straight line where the hardening rate decreases linearly with stress towards a "saturation stress". Stage IV intervenes before the saturation stress is reached and is commonly thought of as another stage of constant, low θ at about $2.10^{-4}\mu$.

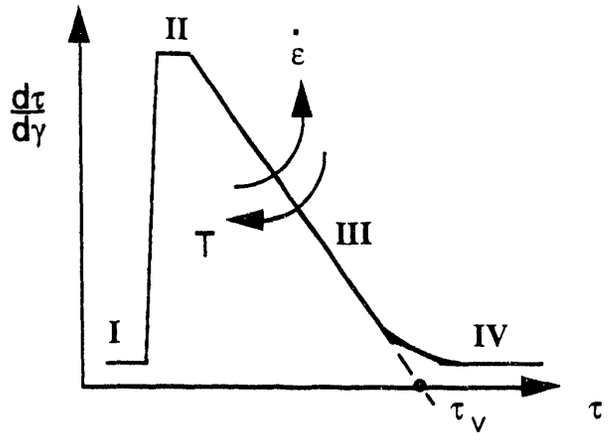

Fig. 2. The Stages of Work Hardening for a single crystal represented on a plot of hardening rate versus flow stress. A polycrystal would show stages III and IV, possibly II also. In stage III, the extrapolation to zero hardening is labeled as τ_v to indicate the Voce stress, and the arrows indicate how the slope varies with increasing strain rate or temperature.

STAGE I: EASY GLIDE

Single crystals of close packed metals will deform on a single slip system with little strain hardening to strains as large as 0.6 when stressed along a crystallographic direction that is not related to the crystal symmetry. This stage of work hardening is known as easy glide, Andrade and Henderson [4], because large amounts of strain can accumulate without much work hardening. The order of magnitude of the work hardening rate is $2.10^{-4}\mu$, where μ is the shear modulus [5] and the flow stress is $10^{-4}\mu$ or less. The end of stage I is not a particularly reproducible phenomenon and is sensitive to material purity and stress raisers on the specimen surface, for example.

The terms "critical resolved shear stress" and "resolved shear strain" have particularly obvious meanings in single slip: the macroscopic stress on the material must be large enough that when the stress is resolved onto the active slip system, a critical shear stress is attained. The scalar ratio between the magnitude of the resolved shear stress and the magnitude of the applied stress is called the Schmid factor, which is a simple function of the single crystal orientation. This same ratio connects the external strain with the shear strain on the active slip system. The shear strain, $d\gamma$ can be written in terms of the mean number of mobile dislocations that traverse the slip plane, dn, and the mean spacing of the active slip planes, d.

$$d\gamma = dn\frac{b}{d} \qquad (1)$$

STAGE I: HARDENING RATE

If each mobile dislocation could pass through the crystal without any portion of it being permanently stopped, the work hardening rate would be exactly zero. The experimental data all show a small but finite work hardening rate which means that some accumulation of dislocation line length occurs. Fourie and Murphy [5] showed by examination in the transmission electron microscope (TEM) that the predominant storage mechanism in stage I is in dislocation dipoles. Parallel edge dislocations of opposite sign that are closer than $\mu b/8\pi(1-\nu)\sigma$, where σ is the current flow stress, form a stable arrangement, Gilman [6].

Argon and East [7] developed a statistical theory for stage I work hardening based on the capture of mobile dislocation segments into dipolar and multipolar configurations. This theory produced the correct order of magnitude and sign of the strain rate sensitivity and temperature sensitivity but over-estimated the work hardening rate by a factor of about 5. It is noteworthy that the low hardening rates observed in stage I are described with fair success by a theory that is based on the accumulation of dislocation debris.

Although stage I is only relevant to single crystal behavior, it is worth noting that the low work hardening rate appears to be a consequence of the accumulation mechanism. That is, dislocation debris in the form of dipoles accumulates which gives a small but finite hardening rate. This hardening rate is of the same order as that observed in stage IV. The combination of low hardening rate and debris accumulation will be taken up again later since a simple quantitative description of stage IV is developed below, based on debris accumulation. It is therefore necessary to understand small strain work hardening behavior in order to make connections to the large strain regime.

TRANSITION TO STAGE II

After a certain amount of strain, single crystals exhibit a transition from a low hardening rate to a much larger rate. This transition is not well defined in terms of either stress or strain and is sensitive to chemical purity, prior handling and stress raisers such as surface blemishes, Nabarro et al. [5]. One might speculate, however, that once dislocation activity on secondary systems has started anywhere in the crystal, autocatalytic propagation occurs, giving rise to stage II.

ATHERMAL HARDENING (STAGE II)

Stage II work hardening was first characterized by an approximately linear stress-strain curve whose slope is an appreciable fraction of the modulus but it was subsequently redefined in terms of an athermal hardening stage [8]. In terms of a resolved stresses and strains, the hardening rate is about $\mu/200$ and has only a mild dependence on temperature or strain rate, Nabarro et al. [5]. The characteristic hardening rate is sometimes less (e.g. $\mu/600$) in b.c.c. metals, however. For a given material, the hardening rate varies only by a factor of 2 with single crystal orientation. It is important to note that this high hardening rate can occur even while a single slip system is supplying the imposed strain. That is, a single crystal can be hardening in stage II while still deforming macroscopically in single slip [9]. Stage II also occurs in tensile tests of <111> oriented single crystals which deform on six slip systems [10], in <100> single crystals which deform on eight slip systems, Hosford et al. [11], and in polycrystals where at least five slip systems must be active in order to accommodate the imposed

strain. The significance is apparent from Burgers vector analysis in the TEM of dislocation structures in single crystals deformed into stage II, Steeds [12]. This shows, surprisingly, high dislocation density on systems other than the primary slip system. What appears to happen is that accumulations of dislocations on the primary slip system leads to the localized production of a critical resolved shear stress on secondary slip systems. This secondary slip presumably relaxes the stress concentration due to pile-ups or concave loops on the primary slip plane but leads in turn to the tangling up of primary with secondary dislocations in an irreversible manner [13].

STAGE II: FOREST THEORY

The consequence of this secondary slip for the flow stress is that the dislocations produced are mostly "forest" dislocations with respect to the primary slip system. The term "forest" refers to the concept that the flow stress on a given slip plane is determined by the short range interaction of mobile dislocations on the slip plane with those dislocations that intersect the slip plane. This theory has been extensively discussed by, e.g., Basinski [14]. It is supported by such experimental evidence as the flow stress in stage I being determined by the density of dislocations that intersect the primary glide plane. That is to say, although a large rise in the density of primary dislocations occurs, the flow stress, σ, hence the hardening rate, $d\sigma/d\varepsilon$, is controlled by the much smaller increase in density of secondary dislocations, see e.g. Argon and Brydges [15]. The forest theory is also supported by experiments on latent hardening [16] where tests of the flow stress on previously inactive slip systems show only small changes in the flow stress from that of the previously active slip system, Basinski and Basinski [17].

The fundamental relationship for flow stress is the Taylor equation,

$$\tau = \alpha \mu b \sqrt{\rho} \qquad (2)$$

Mecking and Kocks [8] reviewed the available data and concluded that equation 2 holds over a wide range of flow stresses and dislocation densities with α=0.5 to 1.0. The term a represents an average interaction strength between dislocations and conceals much of the inherent complexity of detailed dislocation theory. For example, the interactions vary from entirely elastic between dislocations with perpendicular Burgers vectors, to energy storing when intersection leads to formation of a jog. The magnitude of α is significant because if it is too small ($\leq$0.25), dislocations crossing the slip plane will not store any line length [18]: see below for further discussion. Attempts have been made, e.g. Saada [19], to incorporate the details of dislocation interactions into a quantitative theory of work hardening but without notable success. Equation 2 illustrates a fundamental point for comparing flow stresses between materials which is that the shear modulus (μ) is the appropriate quantity to use in normalizing flow stresses. The Burgers vector, b, is also material dependent but varies much less (with temperature) than the shear modulus. The actual flow stress is modified (lowered) by thermal activation, so a more generally useful form of equation 2 includes a temperature and strain rate dependent term; a detailed discussion is not needed here and can be found in, e.g. [8].

MODELS FOR STAGE II

The work hardening rate in stage II is essentially constant. Kuhlmann-Wilsdorf [20] developed a theory for this stage which assumed that the line length of dislocation stored per unit strain is proportional to the reciprocal of the mean free path between existing dislocations,

$$d\rho/d\gamma = k\sqrt{\rho} \quad (3)$$

Given that "self-similarity" holds in the structure, meaning that the constant k in equation 3 is a purely geometrical factor, the above equations can be combined to show that

$$d\tau/d\gamma \approx \mu/200 \quad (4)$$

The factor of 1/200 was the result of arbitrary selection of several geometrical constants. Kuhlmann-Wilsdorf has attempted to extend the mesh-length theory [21] to stage III and even beyond. She assumed, however, that the cell size, which determines the the mesh length, is essentially static in stage III. This assumption is not well founded experimentally as the literature indicates that the cell size varies inversely with the stress or even faster, see e.g. Thompson's review [22]. When strained metals are observed in the transmission electron microscope (TEM), the dislocation substructure frequently is observed to be non-uniform such that the dislocations are concentrated on certain planes. The term "cell" refers to the unit of dislocation structure of order 1 to 10μm that is defined by these planes of stored dislocations.

Other models exist for stage II work hardening which have been well reviewed by Nabarro et al. [5] and by Mitchell [23]. Only one model will be described in detail, however, the Areal Glide Model because this model appears to account for stage II work hardening better than the older models and is not dependent on particular features of the dislocation structure (e.g. a well developed cell structure).

STAGE II: AREAL GLIDE MODEL

The spatial distribution of intersections of forest dislocations with a slip plane makes a crucial difference to work hardening [24]. If the intersections were arranged on a perfect lattice, then at the critical shear stress, a mobile dislocation would be able to shear the whole slip plane. In reality, however, the distribution is non-uniform and yield occurs at a percolation transition. That is, the distance that a mobile dislocation can travel increases very rapidly as the applied stress nears the macroscopic yield stress. A mobile dislocation can cause macroscopic yielding even though it leaves small concave loops behind its passage around local "hard spots". A hard spot corresponds to a local (upward) fluctuation in the dislocation density. Note that a key feature of this approach is that the flow stress is determined by the percolation of mobile dislocations past the hard areas (tangles, cell walls). Because of this, the actual flow stress within the hard spots does not affect the measured flow stress directly, although it does influence it indirectly because it sets the saturation stress ot maximum attainable stress in the material.

A computer simulated microstructure, figure 4, illustrates what happens. An important part of this process is that the concave loops do not remain as Orowan loops, as if the hard spots were impenetrable particles, but instead plastic relaxation occurs. This means that additional dislocations are generated on secondary slip systems so that the concave loop on the primary slip system is converted to dislocation density on other slip systems. Without this relaxation process, tangles would not form because continuing straining would pile up more Orowan loops until enough stress concentration occurred to collapse the innermost loop. At this point dynamic equilibrium has been attained and each new loop will collapse the innermost loop. This leads to an "Areal Glide" theory for stage II work hardening where the development of dislocation tangles develops from the accumulation of concave glide loops around hard spots on a slip plane [13]. The key quantity is the spacing between hard spots, λ, assumed

to be proportional to the current mean spacing of randomly aranged dislocations.

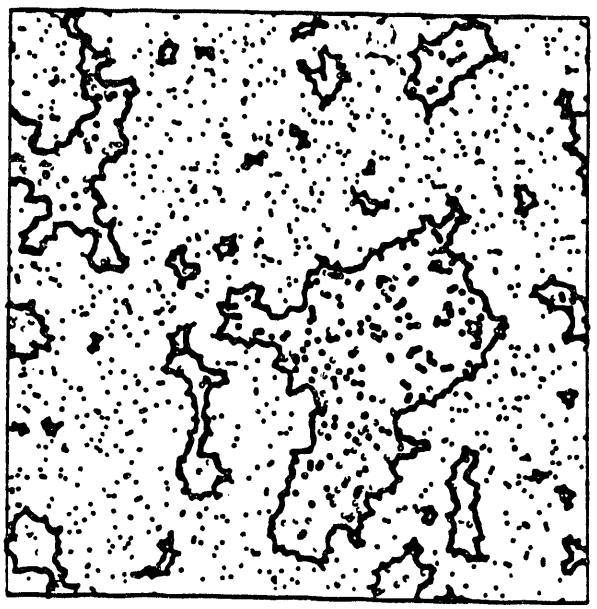

Fig. 4 Concave dislocation glide loops around "hard spots" on a slip plane, from the results of a computer simulation of dislocation glide across a slip plane with a random distribution of point obstacles that represent the intersections of forest dislocations with the slip plane [13].

The constant of order 10 was justified on the basis of computer modeling of dislocation motion through a field of randomly positioned obstacles, representing the intersection of forest dislocations with the slip plane. Then if the passage of a mobile dislocation across the slip plane leaves behind a loop of length $(\sqrt{\rho})^{-1}$ at each hard spot, the strain per loop stored, $d\gamma$, is $b\lambda^2$, giving

$$d\rho/d\gamma = (\sqrt{\rho}\, b\, \lambda^2)^{-1} \qquad (5)$$

from which it can be derived that

$$d\tau/d\gamma = \alpha\, \mu\, /\, (2\, \lambda^2\, \rho) \qquad (6)$$

λ is a small multiple, of order 10, of the mean dislocation spacing $(1/\sqrt{\rho})$ so from equation 5 it follows that the geometrical storage of dislocation line length gives a reasonable value for the hardening rate (in stage II) of about $\mu/200$. The Areal Glide model [13] accounts, for example, for the difference between the observed long slip steps that can be observed on the surface of deformed metals in stage II and the small mean free path for dislocation storage that is required to explain a high work hardening rate.

RECOVERY EXPERIMENTS

Experimental work has been reported by Hasegawa et al. [25] that supports the "two phase" character of slip, i.e. the difference between hard spots on the slip plane where geometrical storage of dislocations occurs, surrounded by softer areas where the mobile dislocations percolate across the slip plane. They measured the change in length during recovery of aluminum samples that had been predeformed in either tension or compression. In both cases the material continued to deform in the same direction as the previous straining though only after an initial reverse straining. Thus a tensile

specimen will first contract (on the order of 0.01%) and then lengthen. The initial reverse straining was ascribed to dislocations running back in the soft regions of their slip planes. The subsequent straining in the same direction as the pre-strain was ascribed to recovery in the hard spots or tangles. The direction of the recovery strain changes sign because the residual stress on each slip plane (on removing the applied stress that accomplished the pre-strain) is negative in the soft regions though still positive in the hard spots. Stated in another way, the fact that there is a measurable, signed strain during thermal recovery indicates that the dislocation networks stored during monotonic straining are polarized.

STAGE III: DYNAMIC RECOVERY

Stage III is characterized by a hardening rate that decreases monotonically with increasing flow stress, leading to the much repeated term "parabolic hardening" for the stress-strain curve. Such a $\sqrt{\varepsilon}$ dependence of the flow stress can rarely be made to work well over a wide range of strain, however. In contrast to the athermal storage of dislocation line length in stage II, stage III behavior is highly temperature sensitive and somewhat strain rate sensitive. Stage III is associated with "dynamic recovery" which means the recovery or loss of line length during plastic straining and which is generally only weakly time dependent. The time dependence can be stated more strongly than this because the rate of recovery is much greater than would occur by static recovery at the same temperature. Dynamic recovery is distinct from the time-dependent kinetics associated with static recovery during annealing treatments. This distinction will be seen to be important in subsequent discussions of large strain models of work hardening. The availability of a model for stage III constructed from first principles of dislocation properties is perhaps even more remote than for the previous stages of work hardening.

THE STAGE II-STAGE III TRANSITION:

In polycrystalline aluminum at room temperature, for example, stage III is the only observable stage of work hardening. At lower temperatures, however, stage II can be observed in aluminum, Hosford et al. [11]. Haasen pointed out [26] that the temperature dependence of the the stress at which stage III starts can be modeled by

$$\log(\sigma_{III}) = A - BT. \qquad (7)$$

This is consistent with a model for thermally activated constriction of dissociated screw dislocation segments so that they can then cross-slip, Schoeck and Seeger [27]. Cross slip permits the oppositely signed screw segments of dislocation loops in different slip planes to annihilate each other and is therefore one of various possible dynamic recovery mechanisms. The current flow stress enters through the fact that the applied stress can assist the constriction process, thereby lowering the apparent activation energy for the process. The activation energies determined from the experimental data for Cu and Ni by Haasen were of the correct magnitude. The presumption is that once cross-slip can occur at a high enough rate, dynamic recovery will begin. It is important to note however, that if work hardening models are constructed on the basis of a single dislocation phenomenon such as cross slip, the models will not fit all the experimental facts. For example, the lack of strong orientation dependence of the work hardening rate in either stage II or III militates against any one mechanism being dominant. The justification of this remark is that different orientations should mean that a different type of dislocation-dislocation interaction is dominant, see e.g. Schwink and Gottler [28].

THE END OF STAGE III

The experimental evidence from much stress-strain data taken out to moderately large strains shows that the work hardening rate in stage III decreases monotonically towards an apparent saturation stress. Accurate descriptions of stress-strain curves have been a topic of discussion for many years but we will not attempt to discriminate between the many competing models in detail. Suffice it to say that the common power law relation has many times been shown to be adequate for only the limited range of the tensile test, e.g. Dorn et al. [29]. Voce [30] and Palm [31] published an alternative exponential stress-strain law that has the advantage of showing an asymptotic saturation stress. The differential form is

$$\theta = \theta_0 (1 - \tau/\tau_v) \qquad (8)$$

where the strain does not enter the relation explicitly. The key modification of this equation for large strain description is to make τ_v (see figure 2) a quantity that increases (slowly) with strain instead of being constant for the particular combination of material, strain rate and temperature. Therefore it is useful to review the theoretical and experimental basis for equation 8.

DISLOCATION MODEL FOR STAGE III

The variation of the apparent saturation stress with temperature and strain rate in aluminum [32] can be modeled with the same dislocation kinetics apply to this as was found for the transition to stage III, equation 2. The physical basis for the Voce-Palm relation and the temperature dependence is as follows.

If the geometric dislocation storage described for stage II continues unabated throughout stage III, the falling hardening rate implies an ever-increasing dynamic recovery rate. A simple assumption that can be made is that the amount of dislocation line length that is lost per unit strain is proportional to the current dislocation density, i.e. everywhere in the structure, stored lengths of dislocation are able to break past their pinning points and be recovered. Quantitatively,

$$d\rho/d\gamma = -L\,\rho \qquad (9)$$

By differentiating equation 2, and combining with equations 3 and 9, one obtains this.

$$\frac{d\tau}{d\varepsilon} = \frac{k\alpha\mu b}{2} - \frac{L\tau}{2} \qquad (10)$$

which is equivalent to equation 8 above, i.e. $\theta_0 = k\alpha\mu b/2$ and $\tau_v = k\alpha\mu b/L$. The physical picture is that the saturation stress is determined in the hard spots where tangles form. The equation that describes the variation of the saturation stress is, by analogy with one form of stress-assisted, thermally activated motion of dislocations at a given structure,

$$\ln\left(\frac{\tau_v}{\tau_{v0}}\right) = -\frac{kT}{A}\ln\left(\frac{\dot{\varepsilon}_0}{\dot{\varepsilon}}\right) \qquad (11)$$

where $\dot{\varepsilon}_0$ is a reference strain rate, τ_{v0} is the (extrapolated) saturation stress at zero Kelvin, and A represents an activation energy, or more correctly an activation work. The reason for the analogy is that, unlike the case of the stress at which stage III commences, Haasen [26], the saturation stress is a result of the evolution of the dislocation structure, not the behavior of a fixed structure. The values of A reported [32] for aluminum corresponded to a low activation energy, approximately $\mu b^3/9$. Therefore

equation 11 is a phenomenological description of thermal activated dynamic recovery that does not attempt to identify a particular controlling dislocation-dislocation interaction.

Equation 11 suggests that the strain rate sensitivity of the saturation stress obeys a power law relationship between stress and strain rate. There are two important differences between this relationship and those derived on the basis of diffusionally controlled recovery, examples of which are discussed below. One difference is that the exponent, n, in the power law relation, decreases linearly with temperature rather than being fixed by the diffusion mode considered, Eq. 12.

$$\left(\frac{\dot{\varepsilon}_0}{\dot{\varepsilon}}\right)=\left(\frac{\tau_v}{\tau_{v0}}\right)^n, \quad n=A/kT \tag{12}$$

The second difference is that at low temperatures, the exponent, n, is very much higher than any possible exponent for a relation derived on the basis of diffusional recovery. For aluminum at room temperature, for example, the data [32] indicates that n~16. Note that other physically-based relationships are possible. Kocks and Chen [33], for example, have recently analyzed the stress-strain behavior of copper over a wide range of temperature and strain rate by applying the same obstacle profile to dynamic recovery as has been previously applied to thermal activated flow stresses.

Mecking et al. have investigated the application of this analysis to a number of f.c.c. metals tested over a wide range of temperatures [34]. They were able to show that Eq. 12 applied over a remarkably wide range of homologous temperatures and also that the differences between materials could be accounted for with a single parameter that varied in the same way as the ratio of stacking fault energy to shear modulus and Burgers vector. This scaling by the stacking fault energy is reasonable since it strongly influences the spacing between pairs of partial dislocations which in turn controls the breaking stress of attractive junctions, or the activation energy for cross slip.

STAGE III: A PHYSICAL PICTURE FOR THE SATURATION STRESS

Starting with the Areal Glide model of stage II work hardening, dislocation storage occurs at the hard spots in the microstructure. These hard spots develop into the cell walls typically observed as straining proceeds. As the rate of dynamic recovery increases in stage III, so a larger and larger fraction of dislocation segments stored in the hard spots or tangles can be recovered. The stored dislocation segments have a spectrum of lengths. The longer the segment, the smaller the (local) stress that is required to bow it out and recover it. As the flow stress rises as a consequence of strain hardening so the mean length of stored dislocation segment will decrease. The saturation stress is therefore determined by the longest dislocation segment that will not be recovered at the applied temperature and strain rate. A more detailed picture can be found in the statistical treatment of dynamic recovery [8].

STAGE IV / LARGE STRAINS

A complete review of large strain experiments was provided by Gil-Sevillano et al. [35] to which the reader is referred for complete lists of references to large-strain studies. The classical large strain metal working process is rolling and the development of large strain studies began with tensile tests of rolled sheet. Such tests have obvious drawbacks: one, there is a major change of deformation mode in going from plane strain compression to tension in the subsequent test; two, there is generally a large change in strain rate from the typically greater than 1 s^{-1} (von Mises equivalent) strain

rate of the rolling passes to the less than 10^{-4} s^{-1} rate of typical tensile tests; three, the stress-strain curve that is generated is discontinuous. In the oft-cited work of Langford and Cohen [3], wire drawing was used to attain large strains and the composite stress-strain curve was rendered nearly continuous by careful tensile tests in which the effects of necking were taken into account. Therefore there was little strain path change between the wire-drawing and the subsequent tensile tests. The main result of their work was that hardening persists, albeit at a low level, to strains as high as 10 without any sign of saturation of the flow stress. Some years before this, Kovacs and Feltham [36] published continuous stress-strain curves obtained from torsion experiments on Ni and Ag which showed a clear stage IV for the Ni, albeit to a smaller strain. Over the years many causes for the sustained hardening observed in stage IV have been proposed. Mecking and Grinberg [37] listed eight possible causes of stage IV (grain size; deformation bands; surface effects; stress induced transformations; changing strain path; plastic instabilities; texture; second phase particles), none of which, however, are causes of stage IV [38]. The work of Rack and Cohen [39] on iron alloys demonstrated that the stage IV work hardening was essentially unaffected by alloying though the flow stress level at a given strain generally increased with alloy content. The same conclusion can be drawn from the more recent work by Hughes [40] on Ni alloys. The effect of strain rate on strain hardening was investigated by performing torsion tests at different constant strain rates at various temperatures [41]. Stage IV in commercial purity aluminum at room temperature, appears to be little affected by strain rates that vary over four orders of magnitude. This suggests that the strain rate sensitivity of work hardening in stage IV is comparable to that at smaller strains.

STAGE IV: TEMPERATURE

Alberdi performed large strain torsion tests on copper [42] at five different temperatures. Plots of hardening rate versus stress show clear transitions from stage III behavior to stage IV behavior at all temperatures, despite the fact that the stage III behavior deviates from a linear decrease of θ with σ at higher temperatures. Extrapolation of the stage III behavior to zero hardening rate yields the same exponential dependence, equation 12, of nominal saturation stress on temperature as discussed above. The work hardening rate and stress at which the transition to stage IV occur both decline slowly with increasing temperature. Embury and Mecking [43] suggested a criterion for the transition of the form

$$\theta_{IV} = c\,\sigma \qquad (13)$$

where θ_{IV} is the work hardening rate at which the transition to stage IV occurs, not necessarily the work hardening rate in stage IV. This criterion is represented on figure 5 as a straight line with c=0.05 and appears to fit the data reasonably well for commercial purity aluminum tested at a variety of temperatures [41]. Embury and Mecking [43] noted the similarity of this criterion to those for diffuse necking, $\theta=\sigma$, and local necking, $\theta=0.5\sigma$, and speculated that stage IV might be associated with microscopic instabilities such as the microbands commonly observed large strains in copper. The onset of instabilities in plastic deformation generally results in reduced load carrying capacity in the material, however, whereas stage IV definitely results in increased load bearing capacity.

STRAIN RATE SENSITIVITY AT LARGE STRAINS

The data on strain rate sensitivity for copper [42], nickel [40] and aluminum [41] show that at low homologous temperatures, the evolution of the strain rate sensitivity is a smooth function of flow stress; no marked discontinuities are present at the transition from stage III to stage IV until the deformation temperature is well above 0.3Tm. The significance of this is that stage IV occurs without marked changes in the character of obstacles to dislocation movement. If, for example, stage IV were due to the accumulation of very small obstacles such as vacancies or vacancy clusters, these obstacles should be surmountable by thermal activation. The strain rate sensitivity would then be expected to rise significantly in stage IV. Large obstacles to dislocation motion such as low-angle boundaries, however, are not surmountable by thermal activation and so should not contribute to the rate sensitivity of a material.

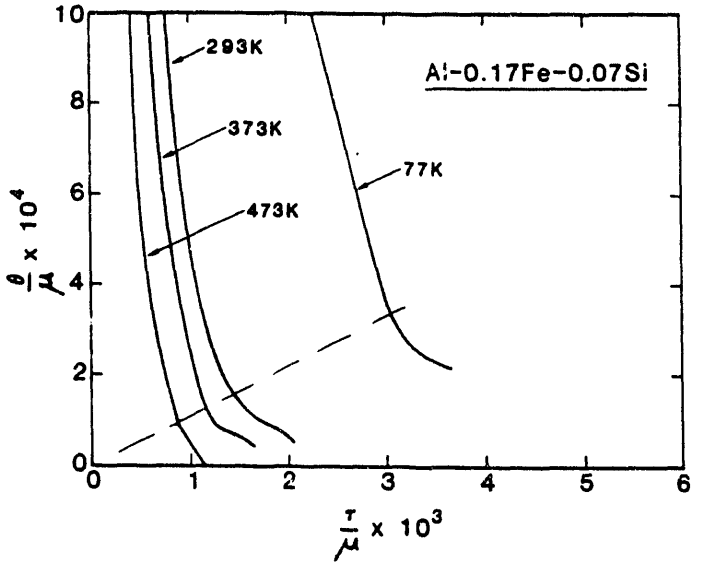

Figure 5. Plot of reduced hardening rate versus flow stress for commercial purity aluminum, tested at four different temperatures.

MODELS FOR STAGE IV

Several models have been proposed for large strain stress-strain behavior by Nix et al. [44], Haasen [45], Zehetbauer [46] and Prinz and Argon [47]. These models employ a "two-phase" structure model where each mobile dislocation must pass through both the soft and the hard parts, "phases", of the structure. Whereas the Voce-Kocks model for the effect of dynamic recovery on work hardening rate predicts a linear decrease of hardening rate with increasing stress, both the Nix and the Prinz models show a less rapid decay of hardening rate. These models, however, do not predict the sharp transition from stage III to IV that is sometimes observed experimentally. The model for stage IV presented here is based on the generally observed fact that plastic straining at low temperatures leads to the accumulation of dislocation debris such as dipoles and loops [48], in addition to the dislocation monopoles, which are usually arranged in tangles or cell walls. The accumulation of dipolar debris may occur as part of the glide process and it may occur as part of the dislocation rearrangements due to dynamic recovery. However, the rate of dislocation rearrangement inside the tangles or loose

cell walls is expected to be affected by the debris left there as a consequence of previous rearrangement processes.

The mechanism of dynamic recovery has been discussed in detail previously [13]. The tangles, which were originally formed by statistical storage of mobile dislocations, have forward internal stresses within them that lead to rearrangement or even annihilation of dislocation segments in this region, thus gradually transforming the tangle into a cell wall. The rate of rearrangement depends on the relative magnitudes of the total local stress and local resistance, such as the breaking strength of attractive junctions as modified by thermal activation. The latter quantity has the effect of a "saturation stress": when the total local stress is equal to it, no further net accumulation can occur. It is this "saturation stress" (defined in the monopole structure) which may be affected by local dislocation debris accumulation.

A useful starting point for a quantitative model is the Voce description of hardening in stage III, equation 8. Now, however, we define τ_{v1} as the saturation stress that would be obtained by extrapolating low-strain data to a zero work hardening rate. Note that, unlike the normal Voce formulation in which τ_v is a constant for a particular choice of strain rate and temperature, here we allow τ_v to vary as deformation proceeds. The second term in parentheses describes the effect of dynamic recovery whereby dislocation line length is lost from the stored dislocation structure. The particular choice of function depends on the accuracy of fit desired to any particular set of experimental data, see [49]. For the purposes of this article, however, we will use the relatively simple formula due to Voce. Starting with the standard relation between flow stress and dislocation density, equation 2, we obtain the rate of loss of dislocation density by combining this with the Voce equation above.

$$\frac{d\rho^-}{d\gamma} = \frac{2\tau}{(\alpha\mu b)^2}\theta_0\frac{\tau}{\tau_{v1}}. \tag{14}$$

Now we describe the relationship between the loss of dislocation density due to dynamic recovery and the rate of accumulation of debris in the tangles. It is reasonable that the debris accumulation should be a fraction, f, of the dynamic recovery rate, which allows us to write:

$$d\rho^+_{debris} = f d\rho^-_{disl.}. \tag{15}$$

A crude estimate of the fraction can be made by noting that the ratio of the dislocation spacing for dipole capture to the mean dislocation spacing is:

$$\frac{\mu b}{8\pi(1-\nu)\tau} : \frac{\alpha\mu b}{\tau}. \tag{16}$$

Numerically this is approximately 0.13, and a further factor of two should be included to account for the complete annihilation of screw dislocations by cross slip. Therefore the upper limit on the fraction of dynamic recovery events that give rise to stored debris is of order 1 in 15.

Now we write for the accumulation rate of debris that

$$\frac{d\rho^+_{debris}}{d\gamma} = f\frac{2\tau}{(\alpha\mu b)^2}\theta_0\frac{\tau}{\tau_{v1}} \tag{17}$$

If the effect of the accumulating debris is to raise the flow stress within the hard regions (tangles, cell walls) of the dislocation substructure then a detailed model is needed for the combined effect of the two components The superposition of flow stress contributions has been examined, e.g. Kroupa [50], but for now we will simplify the model by writing the limiting flow stress in the tangles as

$$\tau_v = \alpha\mu b\sqrt{\rho_{disl.} + \rho_{debris}} \tag{18}$$

which is differentiated to give

$$\frac{d\tau_v}{d\rho_{debris}} = \frac{0.5\alpha\mu b}{\sqrt{\rho_{disl.} + \rho_{debris}}} = \frac{0.5\ (\alpha\mu b)^2}{\tau_v} \tag{19}$$

Assuming that $d\tau_v/d\gamma = d\tau_v/d\rho_{debris} \times d\rho_{debris}/d\gamma$, similarly as above, then

$$\frac{d\tau_v}{d\gamma} = f\theta_0 \frac{\tau^2}{\tau_v^2} \tag{20}$$

but in stage IV, the flow stress is nearly equal to the (current) limiting stress, τ_V. Therefore

$$\frac{d\tau_v}{d\gamma} \approx f\theta_0 \tag{21}$$

This suggests that stage IV will intervene at, and remain constant at 0.07 of the stage II work hardening rate or 3.10^{-4} of the shear modulus, given the above estimate of the factor f. This is in reasonable accord with the experimental observation of stage IV at 2.10^{-4} of the shear modulus. Note that a second order differential equation has been set up here by combining equations 8 and 20, which allows for an indirect effect of debris on the flow stress via the current limiting flow stress.

The hardening behavior can be depicted by using a simple computer program to calculate stress-strain curves. In this program, the Voce law is used, as described above, but the saturation stress is varied using different models for the effect of debris accumulation. Setting the microstructural factor to unity yields the behavior depicted in figure 6. Note that the hardening rate at the onset of stage IV is constant with initial saturation stress and that no further decrease in hardening rate occurs. The transition into stage IV is quite sharp, as observed experimentally, at least at low temperatures. Other models for stage IV that rely on a two-phase structure appear to show a much more gradual transition into stage IV from stage III.

This upper limit, however, is expected to be modified by microstructural variation; that is to say, as the cell wall (tangle) structure becomes more developed at higher strains (and at higher deformation temperatures), it occupies a progressively smaller volume fraction of the material. Therefore the actual fraction should decrease as the cell structure is refined. This suggests that the fundamental relationship between dynamic recovery and debris accumulation could be described as follows, in which ϕ expresses the microstructural effect on the volume fraction of material available for debris accumulation. Both f and ϕ have a range of 0 to 1.

$$d\rho^{+}_{debris} = f\phi d\rho^{-}_{disl.} \tag{22}$$

Experience indicates that the variation with temperature causes the greatest variation in dynamic recovery behavior and therefore cell structure, setting aside alloys for the moment. A plausible description of the fraction, then, reduces the fraction by an multiplier that decreases with temperature, for example, the stage III saturation stress.

$$d\rho^{+}_{debris} = f\frac{\phi\tau_{v1}}{\mu}d\rho^{-}_{disl.} \tag{23}$$

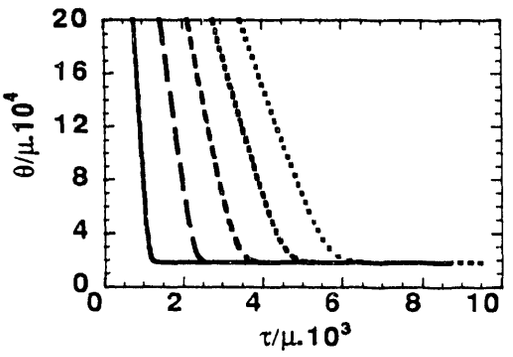

Fig. 6. Variation of hardening rate with flow stress for model based on continuous accumulation of debris from dynamic recovery events.

In this relation, ϕ is chosen such that the product $\phi\tau_{v1}/\mu$ ranges from 0 to 1. In order to illustrate how this microstructural influence can affect the hardening behavior, we write ϕ as a function of strain as follows.

$$\phi = \exp-\left\{\gamma/\Gamma\right\} \tag{24}$$

In this relation, Γ characterizes the rate at which the microstructural factor, ϕ, decreases with strain. The larger Γ, the more slowly the cell structure sharpens. If Γ is related to the strain rate and temperature at which a test is performed in a similar manner to the model above, it is reasonable to assume that it decreases as the temperature is increased or as the strain decreases.

$$\phi|_{\gamma=0} = \frac{A\tau_{v1}}{\mu} \tag{25}$$

In this way, not only does the microstructural factor vary with deformation conditions at the transition to stage IV, but also the factor continues to decrease during continued deformation. This reflects the progressive sharpening of the cell or sub-grain structure in aluminum at ambient temperatures in contrast to the slow progression at low temperatures. Theoretical predictions of hardening behavior with the computer program show a nearly constant hardening rate at the transition into stage IV but a more rapid decrease in hardening at smaller stresses, representing the lesser effect of stage IV at higher deformation temperatures. The most realistic model is a combination of the above, however, in which both the initial value of the microstructural factor varies with deformation conditions, and it decreases with strain.

$$\phi = \frac{A\tau_{v1}}{\mu} \exp - \left\{ \frac{\gamma}{\Gamma} \right\} \qquad (26)$$

This model yields the following results, figure 7. The volume fraction variation now leads to a hardening rate at the onset of stage IV that is approximately linear with the flow stress at the transition. Also, the hardening rate in stage IV decreases more rapidly with stress as the transition stress decreases, as has been observed experimentally for the variation of stage IV with temperature in copper [42] and aluminum [this work].

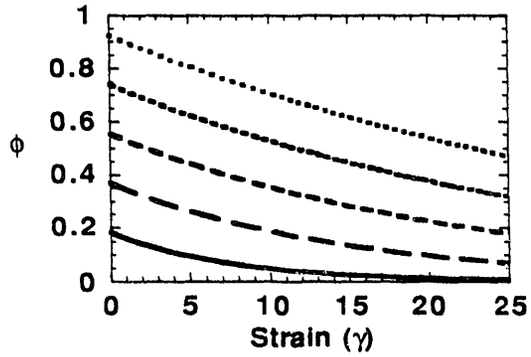

Fig. 7a. Plot of variation of microstructural factor (ϕ) with strain.

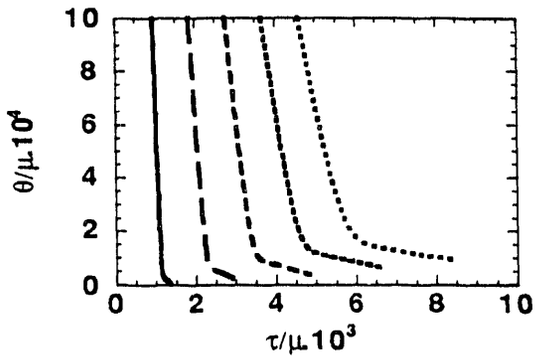

Fig. 7b. Plot of hardening rate versus stress for variation of microstructural factor in (a).

SUMMARY

The various stages of work hardening have been reviewed with an emphasis on the connections between them based on the dislocation storage and recovery mechanisms. Easy glide has a low work hardening rate caused by storage of dislocation dipoles and multipoles on the primary slip system. Athermal work hardening (stage II) has a high work hardening rate caused by storage of dislocation tangles on multiple slip systems and exhibits a self-similar scaling behavior of the dislocation substructure. Dynamic recovery intervenes to lower the hardening rate and this is caused by loss of stored dislocation line length during straining. This stage III of hardening is temperature and strain-rate sensitive because thermal activation assists the dynamic recovery process. The end of stage III appears from small-strain data to be a saturation stress at which there is no net hardening. Another stage (IV) intervenes, however, at low temperatures and hardening can continue at a low level to very large strains. Further decreases in hardening rate during stage IV can be analyzed in the same way as for stage III, leading some authors to postulate a stage V in which dynamic recovery limits stage IV in a manner analogous to stage II/III. Stage IV is caused by the accumulation of dislocation debris, perhaps as a byproduct of dynamic recovery.

REFERENCES

1) Diehl, J., Z. Metall., 1956. 47, 331.
2) Sevillano, J.G., Materials Sci. Forum, 1993. 113-115, 19.
3) Langford, G. and Cohen, M., Trans ASM, 1969. 62, 623.
4) Andrade, E. and Henderson, C., Roy. Soc., Phil. Trans., 1951. 244, 177.

5) Nabarro, F. and Basinski, Z.H., Adv. Phys., 1964. 13, 193.
6) Gilman, J., Discussions of the Fara. Soc., p 123, 1964.
7) Argon, A. and East, G., Trans. JIM (Supplement), 1968. 9, 756.
8) Mecking, H. and Kocks, U. F., Acta Met., 1981. 29, 1865.
9) Kocks, U., Trans. Met. Soc. AIME, 1964. 230, 1160.
10) Kocks, U., Acta Met., 1958. 6, 85.
11) Hosford, W., Fleischer, R., and Backofen, W., Acta Met., 1960. 8, 187.
12) Steeds, J., Proc. Roy. Soc., 1966. A292, 343.
13) Kocks, U. F., Proceedings of the 50th Anniversary Meeting on Dislocations and Properties of Real Materials, publ. Metals Society, London, U.K., 1984. 1, 125.
14) Basinski, Z., Scripta Met., 1974. 8, 1301.
15) Argon, A. and Brydges, W., Trans. JIM, 1968. 9 Supl., 817.
16) Kocks, U. and Brown, T., Acta Met., 1966. 14, 87.
17) Basinski, S. and Basinski, Z., in Dislocations in Solids, F.R.N.Nabarro ed., 1979. 4, 261.
18) Sevillano, J.G., in *Plastic Deformation and Fracture of Materials*, H. Mughrabi, Editor. 1992, VCH, Germany.
19) Saada, G., Acta Met., 1960. 8, 200.
20) Kuhlmann-Wilsdorf, D., Trans. Met. Soc. AIME, 1962. 224, 1047.
21) Kuhlmann-Wilsdorf, D., Met. Trans., 1985. 16A, 2091.
22) Thompson, A., Met. Trans., 1977. 8A, 833.
23) Mitchell, T., 1964. 6, 117.
24) Kocks, U. F., Phil. Mag., 1966. 11, 541.
25) Hasegawa, T., Yakou, T., and Kocks, U. F., Acta Met., 1982. 30, 235.
26) Haasen, P., Phil. Mag., 1958. 3, 384.
27) Schoeck, G. and Seeger, A. in *Report of the Bristol Conference on Defects in Crystalline Solids*. 1955. Bristol, Physical Society.
28) Schwink, C. and Gottler, E., Acta Met., 1976. 24, 173.
29) Dorn, J., Pietrowsky, P., and Tietz, T., Trans. AIME, 1950. 188, 933.
30) Voce, E., J. Inst. Metals, 1948. 74, 537.
31) Palm, J., Appl. Sci. Res., 1947. A1, 198.
32) Kocks, U., J. of Engineering Materials and Technology, 1976. 98, 76.
33) Kocks, U.F., Chen, S.R., and Mecking, H., in *Z. S. Basinski Int. Symp. on Plasticity*. 1992. Kingston, Ont., Canada.
34) Mecking, H., Nicklas, B., Zarubova, N., and Kocks, U. F., Acta Met., 1986. 34, 527.
35) Gil Sevillano, J., Houtte, P., and Aernoudt, E., Progress in Materials Science, 1981. 25, 69.
36) Kovacs, I. and Feltham, P., Phys. Stat. Sol., 1963. 3, 2379.
37) Mecking, H. and Grinberg, A., 5th ICSMA, Int. Conf. on the Strength of Metals and Alloys, P. Haasen et al., eds., 1979. 1, 289.
38) Rollett, A.D., Kocks, U. F., Doherty, R. D. in *Formability and Metallurgical Structure*. 1986. Orlando, FL, TMS, Warrendale, PA.
39) Rack, H. and Cohen, M., Mat. Sci. & Eng., 1970. 6, 320.
40) Hughes, D., Ph. D. thesis, 1986, Stanford.
41) Rollett, A.D., Ph. D. thesis, 1987, Drexel, USA.
42) Alberdi, J., Ph. D. thesis, 1984, Navarra, Spain.
43) Embury, J. and Mecking, H., *private communication*. 1985.
44) Nix, W., Gibeling, J., and Hughes, D., Met. Trans., 1985. 6A, 2215.

45) Haasen, P., J. Phys. France, 1989. 50, 2445.
46) Zehetbauer, M., Acta metall. et mater., 1993. 41, 589.
47) Prinz, F. and Argon, A., Acta Met., 1984. 32, 1021.
48) Fourie, J. and Murphy, R., Phil. Mag., 1962. 7, 1617.
49) Kocks, U.F. in *Ashby Symposium*. 1990. The Mineral, Metals and Materials Society.
50) Kroupa, F., 1964, in"Theory of Crystal Defects", B. Gruber, ed., Academic Press.

END

DATE
FILMED
9/17/93